

1 **Fluorescence screening of collagen preservation in tooth dentine**

2  
3 Andrea Czermak<sup>a\*</sup>, Lothar Schermelleh<sup>b</sup>, Julia Lee-Thorp<sup>a</sup>

4  
5 <sup>a</sup> Research Laboratory for Archaeology and the History of Art, School of  
6 Archaeology, University of Oxford, 1-2 South Parks Road, Oxford OX1 3TG, United  
7 Kingdom

8 <sup>b</sup> Micron Advanced Bioimaging Unit, Department of Biochemistry, University of  
9 Oxford, South Parks Road, Oxford OX1 3QU, United Kingdom

10  
11 \* Corresponding author.

12 *E-mail address:* andrea.czermak@arch.ox.ac.uk

13  
14  
15 Keywords: Dentine microsampling; carbon and nitrogen isotope analysis; collagen  
16 degradation; autofluorescence; fluorescence microscopy

17  
18 Short Communication

19 Graphical Abstract

20 Figures: 3

21 Supplementary Material

22  
23 **Highlights:**

- 24 • Diagenetic changes and the degree of degradation of collagen in tooth dentine can  
25 be effectively monitored by fluorescence microscopy.
- 26 • Autofluorescence can be used to map suitable areas for sampling.
- 27 • Fluorescence imaging is an effective screening method to predict collagen quality  
28 and quantity ahead of sampling.

## Abstract

Isotope analysis of collagen from high-resolution sequential samples of dentine has become a popular tool to provide diachronic insights into individual life histories including childhood diet, stress episodes, and mobility during the tooth formation period. New microsampling approaches improve temporal resolution enabling tracking of diet shifts within relatively short time-spans. These methods, however, necessarily deliver small samples and depend upon good collagen preservation at similar high-resolution scales. Yet present methods indicate state of collagen preservation only *after* sampling and isotope analysis. Here we present a method for prior determination of collagen preservation, based on differential autofluorescence imaging of tooth longitudinal thin sections to map regions of intact and degraded collagen in the corresponding sampling areas. We find that even in dentine areas that were apparently intact based on histology, decay was detected in fluorescence images and that these could be correlated to lower collagen amounts and higher C/N ratios. Areas identified as ‘severely decayed’ dissolved after demineralization. The presented dual-color autofluorescence imaging approach allows determination of areas of degraded collagen at high resolution. This can be used to detect diagenetic changes in collagen ahead of sampling and facilitates selection of well-preserved samples.

## 1. Introduction

The isotopic composition of sequentially sampled small increments of tooth dentine reflects alterations in diet within relatively narrow time-spans during the period of tooth formation. Thus, approaches based on microsampling of dentine are of particular importance to study transitional periods in an individual's life, such as weaning, dietary changes or mobility (e.g. Eerkens et al., 2011, 2016; Beaumont et al., 2013, 2016; Henderson et al., 2014; Sandberg et al. 2014; Beaumont & Montgomery 2015; Fernandez et al., 2018). However, these require destructive sampling, and for the more precise methods that also necessitate sectioning, sample sizes can be rather small (0.5-1.0 mg) and no duplicate measurements are possible (Czermak et al. 2018; Fernandez et al. 2018). Thus, it is important to choose teeth with well-preserved dentine, and to sample intact collagen. While dentine is known to preserve well in the archaeological record under favorable conditions (Kendall et al., 2018), any alteration of the collagen can have an impact on the reliability of the data or even render the measurement of its isotopic composition impossible.

Diagenesis of archaeological bones and teeth has been subject to extensive research, demonstrating that multiple, complex processes are involved (for a recent review see Kendall et al., 2018). Collagen damage leads to a change in its organization (Miles et al. 2000) and composition, partial peptide fragmentation and dissolution, and ultimately to collagen loss (Collins et al. 1995). Changes to collagen may be subtle, resulting in subtly different isotope results. This can be problematic for dentine microsampling approaches attempting to obtain fine-scaled diachronic information about an individual. Alterations, potentially mistaken for real changes, may actually merely reflect preservation.

Collagen type I quality is commonly assessed according to criteria such as measuring the total amount extracted (wt%), %C and %N, and atomic weight C/N ratio. In intact collagen %C values should be ca.  $34.8 \pm 8$  wt%, and %N values 11-16 wt% (van Klinken, 1999, Oxford  $^{14}\text{C}$  database). C/N ratios of 2.8 – 3.6 are normally considered acceptable (e.g. DeNiro, 1985; Ambrose, 1990; van Klinken 1999; France et al. 2014; Madden et al., 2018), although the calculated C/N ratio for intact collagen is 3.2 (Szpak 2011). However, such quality controls can only be applied *after* sampling, demineralization and conducting elemental analysis. Therefore, a reliable screening method to predict collagen quality ahead of sampling is highly desirable.

Conditions that lead to the exposure of collagen in bone and teeth to enzymatic attack, such as acidic soils, microbial fermentation or ‘tunneling-activity’ (Child, 1995), are similar to the process of dental caries (Klont & ten Cate, 1991). Several studies have focused on the evaluation and quantification of diagenetic bone alteration, using microstructural traits to depict the overall preservation of bone tissue (e.g. Turner-Walker et al., 2002; Turner-Walker and Syversen, 2002) and to predict preservation by histological observation of bone (Hedges et al., 1995; Hollund 2012; Kendall 2018) and tooth samples (Hollund et al. 2015).

Fluorescent properties of collagen have been used for the optical investigation of collagen preservation in bones. Hoke et al. (2011) presented an UV-induced screening method of bone cross sections using autofluorescence properties of intact collagen, and an earlier study on compact bone using confocal laser-scanning microscopy reported autofluorescence emission around 525 nm upon excitation with 458 nm laser light associated with poorly preserved areas (Maggiano et al. 2009). Autofluorescence is the natural emission of light by biological substrates when excited within a specific spectrum and is based on the presence of endogenous fluorophores (Bachmann et al. 2006, Croce & Bottiroli, 2014.). Collagen contains several fluorogenic compounds and shows autofluorescence when excited with ultraviolet (UV) light at ~370 nm wavelength, with emission in the blue spectrum at 405-450 nm (Georgakoudi 2002; Lakowicz 2006). Albeit the chemical nature of autofluorescence in human bone and teeth is still not completely understood, fluorescence is apparently triggered by the organic phase, independent from the mineralized phase (Capasso et al. 2017). Autofluorescence in collagen is presumably elicited by cross-links (Armstrong & Horsley 1972), also aromatic amino acids such as hydroxylysine and tyrosine, or glycyl-aspartic acid and glycyl-serine that display emission near the collagen fluorescence peak (Perry & Hefferren 1973; Eyre et al. 1984; Fujimori 1989).

Autofluorescence of teeth upon UV-irradiation was first reported by Stübel (1911). Since fluorescence intensity of carious tooth areas is weaker than that of non-carious (Benedict 1928), carious lesions were detected by using fluorescence as a histological marker (e.g. Hartles & Leaver, 1953; Armstrong, 1963; Foreman, 1980).

As different fluorescence spectra directly reflect sound and carious dentine respectively, autofluorescence can serve as a potential indicator for any application that requires distinguishing intact from degraded collagen. Here a screening method

based on differential autofluorescence mapping is presented that allows visual assessment of collagen preservation in archaeological teeth prior to demineralization. It was prompted by our requirement to identify a developmentally appropriate sampling trajectory prior to demineralization because growth increments are impossible to identify securely afterwards. This screening enables pre-selection of sample areas that contain well-preserved collagen and avoidance of those zones that have poor or even moderately poor preservation. Ultimately, the approach helps to avoid unsuccessful, costly analyses and further destruction of the material.

## **2. Material and Methods**

### *2.1. Material*

Two modern, surgically extracted teeth<sup>1</sup> were used as optical controls for fluorescence microscopy: (1) sound ('positive control') and (2) caries ('negative control'). Five archaeological samples taken from a similar burial environment<sup>2</sup>, were pre-selected based on transmission light images. Optically well-preserved teeth according to transmission light microscopy, but with mixed areas of intact, intermediate and degraded collagen in fluorescence images, were selected for subsequent demineralization and light stable isotope mass spectrometry to test for C/N ratios and isotope compositions. All archaeological samples were taken from a similar burial environment, with tooth A and B being extracted from the same individual.

### *2.2. Sectioning, microscopy and image processing*

Tooth samples were embedded in Herculite II gypsum molding material and bisected longitudinally using a Buehler Isomet low-speed diamond saw with a micrometer gauge, abrasive wafering blade and a cooling water bath. Thereafter, a longitudinal thin section of ~70 µm thickness was taken from one half (central part of the tooth) and mounted on a microscopy slide with Eukitt (Sigma Aldrich).

Consecutive series of 3-channel microscopy images were acquired in a raster ('mosaic') on a GE DeltaVision DV core wide-field epifluorescence microscope using a 4x/0.16NA air UPlanSApo objective (Olympus), Xenon light source, excitation and emission bandpass filter: (1) Transmission light; (2) Filterset A: excitation 360/40 nm (center/ bandpass width), emission: 457/50; (3) Filterset B: excitation 490/20 nm,

---

<sup>1</sup> Modern teeth were provided with patients' consent from a dental surgery in Darmstadt, Germany

<sup>2</sup> Individuals were buried a 5th century AD cemetery (Niedernai, Alsace, France).

emission: 528/38<sup>3</sup>. Image series were stitched to a high-resolution image of the entire tooth section using GE's softWoRx acquisition software to visualize the dentine increments of this section.

Images were processed in ImageJ/Fiji (Schindelin, 2012). First a linear contrast correction was applied (all images same scaling): 12-bit image (0-4096 grey scale levels), followed by: (1) Transmission light: Gamma correction (Filter 0.5-0.7) to enhance the contrast of poorly visible dark areas without saturating the brighter areas; (2) Filter A: min 100, max 1000; (3) Filter B: min 200, max 2000.

Images taken with Filterset A (intact collagen) were pseudo-colored in green, those taken with Filterset B (degraded collagen) were pseudo-colored in red. Images were merged to better distinguish areas with intact dentine from decayed dentin and highlight intermediate degradation stages (see Graphical Abstract and Fig. 1). Based on the merged image these can roughly be grouped into 'green' representing largely intact collagen, 'yellow to orange' representing increasing proportions of degraded collagen versus intact collagen, and 'red' representing fully degraded collagen.

### *2.3 Microsampling and collagen extraction*

From archaeological samples enamel was removed and saved for further analysis and tooth halves were demineralized in 0.5 M hydrochloric acid (HCl) solution at 4 °C for 3-10 days until translucent and flexible. Samples were soaked in deionized water until pH neutral. Demineralized tooth halves were microsampled under a dissecting stereomicroscope (Olympus SZX). The sampling area was sectioned longitudinally on a Harris cutting mat and the posterior side was removed to minimize sampling depth (Guiry et al., 2016), leaving a remaining ~1.5 mm thick longitudinal slice. Samples were taken using a KAI Medical biopsy-punch with plunger (Ø 1.0 mm) (Fernandez et al. 2018) to obtain a dentine micro-cylinder of ca. 1 mm diameter and ~1.5-2 mm length (Fig. 2A). Fluorescence images of the corresponding thin section were used as an optical reference to track collagen preservation of each tooth. Dentine samples were transferred into micro-tubes and lyophilized for 4-6 h. The small solid dentine 'sticks' were weighed and transferred into tin capsules after freeze-drying.

---

<sup>3</sup> Filtersets A and B are commonly used for chemical and biological applications, e.g. to detect the fluorescent dyes DAPI (4',6-diamidino-2-phenylindole, excitation/emission maximum at 358 nm/461 nm) and FITC (Fluorescein isothiocyanate, excitation/emission maximum 495 nm/519 nm), respectively.

Since dealing with very small sample sizes, our collagen extraction strategy was customized. First, a modified *chunk method* (Sealy et al., 2014) was applied, i.e., demineralizing and freeze-drying chunks, skipping gelatinization and ultra-filtration. However, the NaOH step was omitted as described in the *Extraction method C* by Jørkov et al. (2007)<sup>4</sup>. These steps were avoided to minimize collagen loss. To exclude potential humic presence we also tested sample weights at well-preserved and decayed areas with and without applying 0.1 M NaOH 3x20 min on microsamples from the same teeth (Supplementary Analysis S1, Supplementary Table S1, Supplementary Figs. S2 and S3).

#### 2.4. Isotope analysis

Dentine samples were transferred into tin capsules and sorted by mass into three groups: (1) 0.2-0.4 mg; (2) 0.5-0.6 mg; (3) 0.7-0.9 mg. Weights of the standard analyzed alongside the unknowns were adjusted accordingly. Standards were interspersed throughout each mass spectrometry run (~60% samples, ~40% standards). Due to their small size, microsamples were not measured in duplicate. Samples were loaded into a SERCON 20/22 continuous flow isotope ratio mass spectrometer coupled with an elemental analyzer for measurement of carbon and nitrogen isotopes. By convention, stable isotope ratios are expressed in the  $\delta$ -notation, in parts per thousand (per mil or ‰) relative to an international standard, as:  $\delta_x Z = (R_s/R_{ref} - 1) \times 1000$ , where  $Z$  = carbon or nitrogen respectively and  $R$  = isotope ratio ( $^{13}\text{C}/^{12}\text{C}$ ,  $^{15}\text{N}/^{14}\text{N}$ ) and the international standards for  $^{13}\text{C}/^{12}\text{C}$  and  $^{15}\text{N}/^{14}\text{N}$  are Vienna Pee Dee Belemnite (VPDB) and Ambient Inhalable Reservoir (AIR), respectively. Analytical precision for both isotopes is  $\pm 0.2\text{‰}$  ( $1\sigma$ ) based on repeated analyses of internal (alanine, marine seal collagen, bovine collagen) and international standards (caffeine IAEA 600).

Statistical analysis was performed using Microsoft Excel for Mac (Version 16.13) using the Analysis ToolPak. Normal distribution of data was assessed using *Chi-Squared Goodness-of-Fit Test*. Kruskal-Wallis-Test and ANOVA single factor test was used to assess variation in weight, C/N, %C and %N by collagen

---

<sup>4</sup> The term ‘collagen’ as commonly used in many publications, and here, is not entirely accurate, as collagen from the dentine is not ‘extracted’. Type I collagen is the main structural protein in dentine with ~20% of weight, the remainder is non-collagenous proteins (< 5%) (Schroeder, 2000). As other organic compounds are present in lesser proportion, and demineralizing and freeze-drying chunks of well-preserved material without gelatinization shows no difference in the isotope composition (Sealy et al. 2014), therefore the use of the term ‘collagen’ is kept.

fluorescence groups. For testing groups with unequal variance, a t-test (*'two-sample assuming unequal variance'*) was used with a significance level  $<0.05$  for all tests. Correlation coefficient was calculated using the PEARSON function (Bärlocher, 1999).

### 3. Results

Based on the assumption that the autofluorescence properties of dentine collagen may be used to determine the degree of its preservation, we assessed autofluorescence of thin sections from modern, surgically extracted and archaeological teeth. Preceding histologic assessment by transmission microscopy all showed an apparently good preservation state, with only little 'bacterial tunneling' in the archeological samples. Strikingly, when comparing autofluorescence in different wavelength ranges in sections from freshly extracted teeth used as control, a bright and even autofluorescence was observed in the shorter wavelength range (Filterset A: ex. 360/40 nm, em. 457/50 nm; pseudo-colored green), but almost no signal at the longer wavelength range (Filterset B: ex. 490/20 nm, em. 528/38 nm; pseudo-colored red). Notable exceptions were regions with known caries lesions (Fig. 1A). Similar to the control teeth, archaeological samples (Fig. 1B, example teeth A-E) also showed autofluorescence at the shorter wavelengths (Fig. 1B, first column). However, in contrast to modern unburied teeth, autofluorescence at the longer wavelengths was visible across the thin section with varying intensity (Fig. 1B, second column). Autofluorescence was ranging from only little signal (tooth A), different grades of non-homogeneously intense signal e.g. strong autofluorescence surrounding the right root canal (tooth B), the pulp cavity (tooth C) or parts damaged by dental neck caries (tooth D), to autofluorescence accompanied by material loss indicated by voids of signal (tooth E). After the assessment of thin sections, the corresponding tooth halves (Fig. 1B, fourth column) were demineralized. The structure of modern teeth as well as those areas of archaeological teeth that appeared green in the pseudo-colored fluorescence image, representing intact collagen, remained firm. In comparison yellow-colored areas were less firm, but still kept the natural tooth shape, whereas orange and red areas showed a complete loss of structural integrity, i.e. they were no longer pseudomorphs of the original. This was in particular the case for tooth E, which proved impossible to extract samples from due to a complete loss of structure. From these results it was



reasoned that the differential autofluorescence distribution visualized by merging both autofluorescence signals would be a useful indicator for the degree of collagen preservation in different tooth zones or the proportion of degraded collagen respectively. (Fig. 1B, third column). Notably, regions with increased longer wavelength autofluorescence often correspond with reduced shorter wavelength autofluorescence (Supplementary Fig. S4, line plots of tooth B), indicating a transition from a largely intact to a partially degraded state, although differences in general collagen amount and thickness variations across thin sections also affect the absolute intensities and need to be considered.

To test the predictive value of the autofluorescence mapping for collagen preservation, microsamples were taken from different areas of the same tooth, characterized by different autofluorescence distributions. According to the color gradient shown in the merged pseudo-colored fluorescence images, four stages were assigned: (1) green, intact dentine; (2) yellow, early decay; (3) orange, advanced decay; (4) red, severe decay. About 9-14 microsamples were taken from each archaeological tooth with  $n=29$  stage 1 (green),  $n=8$  stage 2 (yellow),  $n=5$  stage 3 (orange), and  $n=6$  stage 4 (red) (Fig. 2A, B). Collagen amount after freeze-drying, C/N ratios, %N and %C, and isotope analyses from samples and their fluorescence stages are shown in Fig. 2C (for comprehensive data see Supplementary Analysis S2 and Supplementary Tables S2-S7).

Significantly less collagen was found in samples taken from orange ('advanced decay') areas (both  $p=0.009$ ) compared to samples taken from green ('intact') or yellow ('early decay') dentine (Fig. 3B). No significant difference in these parameters was detected between samples from green and yellow areas. Samples from red areas yielded 0.1 mg or less dry mass of collagen, or were irretrievable after freeze-drying (Fig. 2C, Fig. 3B). Collagen amount taken from green and yellow areas varies between 0.35 and 0.91 mg. Samples smaller than 0.3 mg, only derived from orange areas, have slightly higher C/N ratios ( $\geq 3.3$ ) than larger samples. A strong correlation between collagen amount and C/N was found ( $r = -0.8$ ). While there is no difference in C/N ratios between samples taken from areas with preservation stage 1 (green) and 2 (yellow), C/N ratios of advanced decayed areas (orange, mean C/N: 3.4) are significantly higher than in intact (green, mean C/N=3.2,  $p=0.003$ ) or slightly degraded areas (yellow, mean C/N=3.3,  $p=0.004$ ).

Only %N is significantly affected by poorer preservation (orange areas), whereas %C is not (Fig. 3A). No significant difference exists between preservation stages and %C, but a difference appears in %N between orange and green, as well as yellow (green:  $p=0.049$  and yellow:  $p=0.047$ ) (Fig. 3A). The proportion of %C to %N seems to be affected only in samples from orange areas, with %N slightly too low (Fig. 3A)<sup>5</sup>. Although having a similar small sample size as some orange samples ( $\approx 0.4$  mg), those yellow and green samples are not affected in C/N (Fig. 2 and Fig. 3A).<sup>6</sup> Notably, all results are within the acceptable ranges for collagen quality control.

Fluorescence screenings as well as quality criteria such as C/N and %N of samples from stage 3 areas (orange) indicate advanced degraded collagen. However, %C seems not affected as well as  $\delta^{15}\text{N}$  and  $\delta^{13}\text{C}$  values that do not differ much from samples taken from corresponding well preserved areas on the opposite root that should have formed at approximately the same time (Fig. 2B, C). Samples after NaOH-treatment show no significant weight loss compared to samples without, confirming that no humic substances were present in our samples (Supplementary Analysis S1).

#### 4. Discussion

Here we introduce a fluorescence-based approach to assess collagen quality from tooth thin sections, prior to microsampling and isotope analysis. Natural dentine when illuminated with light in the visible spectrum (400-630 nm) fluoresces in a broad range between 540-700 nm (Alfano & Yao, 1981; König et al., 1999). For collagen, which constitutes the main organic matrix in dentine, autofluorescence upon  $\sim 370$  nm excitation has been attributed to collagenase digestible collagen cross-links (Kollias et al. 2002). In dental caries autofluorescence properties are most likely elicited from denatured collagen structure. Pentosidine, a glycation end-product after Maillard reaction, is also forming fluorescent cross-link between arginine and lysine residues (Pawlak et al., 2008; Levallois, 2012). Other fluorophores in caries are porphyrines, presumably synthesized by oral bacteria that penetrate dentinal tubules (König et al., 1999). Our images of freshly extracted teeth with intact dentine show intense autofluorescence at shorter wavelengths (Filterset A: ex. 360/40 nm, em. 457/50 nm),

<sup>5</sup> Linear regression green:  $y = 3.1091x - 4.9919$   $R^2 = 0.7583$ ; linear regression yellow:  $y = 2.777x - 0.0117$   $R^2 = 0.7024$ ; linear regression green and yellow:  $y = 3.031x - 3.8283$   $R^2 = 0.73954$ ; linear regression orange:  $y = 2.0512x + 10.889$   $R^2 = 0.3179$ . For diagrams see Supplementary Material.

<sup>6</sup> Green samples: A9, B5, B6; yellow samples: C1, C8, D2;

but no signal at longer wavelengths (Filterset B: ex. 490/20 nm, em. 528/38 nm). Notable exceptions are regions with small caries lesions, indicating locally confined collagen degradation. Bacteria most commonly associated with dentine caries have no significant autofluorescence in the longer excitation-emission range of Filterset B (König et al., 1993) and can thus be excluded as its source.

Similar to the freshly extracted teeth, intact dentine in archaeological samples autofluoresces at shorter wavelengths but not at longer wavelengths, whereas areas with degraded dentine can be identified by autofluorescence at longer wavelengths. In those regions, autofluorescence is typically reduced in the shorter wavelength range, indicating a shift from intact to degraded collagen. A total loss of collagen is indicated by absence of any autofluorescence (tooth E). Merged autofluorescence images of archaeological samples thus enable to clearly distinguish zones of well-preserved collagen from areas of early, advanced and severely decayed collagen, as confirmed by the structural assessment of demineralized tooth-halves. Demineralization of well-preserved tooth dentine yields a collagen ‘pseudomorph’ which keeps the same shape and almost the same size as the original tooth. Accordingly, the structure of freshly extracted demineralized teeth was firm. In our archaeological samples, poorly preserved teeth or tooth areas became somewhat amorphous and depending on the degree of decay dissolved partially in HCl, which made microsampling more difficult or even impossible.

Importantly, the information obtained from differential autofluorescence screening was in good agreement with collagen amounts and C/N ratios. Collagen amounts obtained from samples of approximately the same size differed depending on the fluorescence stage of the sampling area. Samples taken from areas of fluorescence stage 1 (green) and 2 (yellow) contained sufficient amounts of collagen for isotope analysis and also met commonly accepted quality standards (C/N, %C and %N). Samples taken from lower preservation areas contained significantly less collagen. While stage 3 areas (orange) still yielded enough material for analysis, collagen amounts of stage 4 areas (red) were 0.1 mg, less, or even none. Samples as small as 0.35 mg still delivered acceptable results according the %C and %N quality criteria.

Autofluorescence-screenings clearly identify zones containing degraded collagen to a different degree (yellow, orange and red). The results correspond well with traditionally measured parameters, such as weight loss or C/N ratios. All zones

in archaeological dentine yielded C/N ratios that would fall into the conventionally accepted ranges (e.g., DeNiro, 1985; Ambrose, 1990; van Klinken, 1999; France et al. 2014; Madden et al., 2018). Isotopic compositions of well-preserved (green) and slightly degraded (yellow) areas had almost ideal C/N ratios, confirming the appropriateness of the established C/N ratio range criteria for well-preserved collagen. From the more degraded areas (orange) smaller sample sizes (<0.35 mg) could be obtained, which typically gave higher C/N ratios (>3.3). However, even in these less-well preserved areas, collagen within the accepted C/N-range (2.8–3.6) could be extracted.

Relatively poor preservation had little effect on %C, whereas %N values were lower in samples taken from degraded (orange) areas (Fig. 3A, B). Low %N is an indicator for protein degradation (De Niro, 1995), however, Jacob et al. (2018) suggest samples with lower %N in bone may still yield sufficient collagen for isotope analysis. A positive correlation between fluorescence intensity and dentine nitrogen concentration in sound dentine has been reported previously (Armstrong, 1963). Thus, the observed yellow and orange color in merged fluorescence images in this study may also be caused by protein degradation induced reduction in nitrogen content lowering autofluorescence in Filterset A. It is more likely, however, that the differences in C/N ratios between the green/yellow and orange areas are due to the low sample mass (<3.5 mg) and the limited sensitivity of the mass-spectrometer, also resulting in lower %N. Furthermore, the small sample numbers, especially those taken from orange areas, do not allow for meaningful statistical comparisons.

Contamination with humic substance could also contribute to relatively high C/N ratios. These dark colored compounds present in soil can infiltrate bone and tooth and link to collagen. They are carbon rich and nitrogen poor, relative to collagen, with low  $\delta^{13}\text{C}$  values since derived from decaying organic matter. Thus, contamination with humic substance can cause relatively high %C and C/N ratios (Szpak et al. 2017). In addition, humic substances can also cause a strong fluorescence (peak excitation: 465-475 nm, peak emission: 509-515 nm) (Hayase & Tsubota, 1985; Boudin et al., 2011). Since degraded collagen (caused by caries or decay) and humics fluoresces in the same excitation/emission range, areas highlighted by Filterset B (red) contain either altered collagen and/or are contaminated with humics. Based on visual inspection (no brownish color), humic contamination seemed to be absent. However,

since a NaOH-step was omitted, the possibility of humic contamination remained. NaOH treatment it is not common practice in dentine microsampling protocols and often omitted to avoid collagen loss (e.g. Henderson et al., 2014; Sandberg et al., 2014; Beaumont et al., 2016; Fernandez et al., 2018), although few studies include this step (Eerkens et al., 2011, 2016; Burt et al., 2015). Recently van der Haas et al. (2018) demonstrated that a 6-hour base-wash does not cause material loss in archaeological microsamples. Here, no significant weight difference was observed between samples after 3x20 min 1M NaOH-treatment (Szpak et al. 2017) and untreated samples taken from any fluorescence area, confirming that (1) a base-wash can be applied on microsamples without significant material loss and (2) the possibility of humics contributing to the observed autofluorescence in the analysed samples can be excluded. Besides, although %C and C/N-ratios are slightly higher in samples from orange areas,  $\delta^{13}\text{C}$ -values are relatively low and similar to those taken from neighboring green areas, which also renders humic contamination unlikely.

Poor preservation leads to small sample size with slightly increased C/N-ratios. Degraded areas, however, still retained unaltered collagen that showed chemical and isotopic integrity. This observation is consistent with findings by Collins et al. (2002) that parts of the bone unaffected by zones of deterioration may still retain intact biomolecules. Considering the weight loss of the samples, degraded collagen fraction presumably removed during the extraction process, while collagen present even in advanced degraded areas can still be used for isotope analysis. In fact, samples taken from orange areas can still produce good quality data, albeit at the expense of requiring bigger sample sizes which compromises temporal resolution. Thus, fluorescence-screening allows to adjust sample sizes in advance. Samples consisting mainly of red areas, however, will provide no intact collagen at all and further destruction of the material is not worthwhile.

In conclusion, the degree of degradation of collagen can be effectively monitored by fluorescence microscopy. The distinct autofluorescence properties of intact and (even mildly) degraded collagen, as well as potential contamination with humic substances can be used to detect diagenetic changes before sampling, demineralization and mass spectrometry. The proposed dual-color autofluorescence imaging approach can monitor early decay in collagen at the histological scale and

facilitates selection of well-preserved samples or sampling areas for bio-archaeological analyses where intact collagen is required.

#### *Acknowledgements*

We are grateful to Peter Ditchfield (University of Oxford) for technical support with mass spectrometry and Sylvia Stang (Dental Surgery, Darmstadt) for providing material. This research was funded by the German Research Foundation (DFG) and the Agence Nationale de la Recherche (ANR) as part of the NiedArch's collaborative research project (principal investigators: Susanne Brather-Walter and Eckhard Wirbelauer). We would like to thank the reviewers who helped to significantly improve this manuscript.

#### **6. Supplementary Material**

- Supplementary Analysis S1. Sodium hydroxide (NaOH) treatment
- Supplementary S2. Calibration and Analytical Accuracy
- Supplementary Analysis S3. Intensity profile plot analysis
- Supplementary S4. Additional data plots

## 5. References

- Alfano, R.R. and Yao, S.S., 1981. Human teeth with and without dental caries studied by visible luminescent spectroscopy. *Journal of Dental Research* 60 (2): 120-122.
- Ambrose, S.H., 1990. Preparation and characterization of bone and tooth collagen for isotopic analysis. *Journal of Archaeological Science* 17(4): 431-451.
- Armstrong, W.G., 1963. Fluorescence characteristics of sound and carious human dentine preparations. *Archives of Oral Biology* 8: 79-90.
- Armstrong, W.G., Horsley, H.J., 1972. Isolation and properties of fluorescent components associated with calcified tissue collagen. *Calcified Tissue Research* 8 (1): 197-210.
- Bachmann, L., Zezell, D.M., Ribeiro, A.D.C., Gomes, L., Ito, A.S., 2006. Fluorescence spectroscopy of biological tissues – a review. *Applied Spectroscopy Reviews* 41 (6): 575-590.
- Bärlocher, F., 1999. *Biostatistik – Praktische Einführung in Konzepte und Methoden*. Thieme Verlag, Stuttgart, New York.
- Beaumont, J., Gledhill, A., Lee-Thorp, J.A., Montgomery, J., 2013. Childhood diet: a closer examination of the evidence from dental tissues using stable isotope analysis of incremental human dentine. *Archaeometry* 55: 277-295.
- Beaumont, J., Montgomery, J., Buckberry, J., Jay, M., 2015. Infant Mortality and Isotopic Complexity: New Approaches to Stress, Maternal Health, and Weaning. *American Journal of Physical Anthropology* 157 (3): 441-457.
- Beaumont, J., Montgomery, J., 2016. The Great Irish Famine: Identifying starvation in the tissues of victims using stable isotope analysis of bone and incremental dentine collagen. *PLoS one*: 11(8): e0160065.
- Benedict, H.C., 1928. A note on the fluorescence of teeth in ultra-violet rays. *Science* 67: 442.
- Boudin, M., Boeck, P., Vandenabeele, P., Mitschke, S., Van Strydonck, M., 2011. Monitoring the presence of humic substances in wool and silk by the use of non-destructive fluorescence spectroscopy: quality control for <sup>14</sup>C dating of wool and silk. *Radiocarbon* 53 (3), 429-442.
- Capasso, L., D’Anastasio, R., Guarnieri, S., Vicianoa, J., Mariggìò, M., 2017. Bone natural autofluorescence and confocal laser scanning microscopy: Preliminary results of a novel useful tool to distinguish between forensic and ancient human skeletal remains. *Forensic Science International* 272: 87-96.
- Child, A. M., 1995. Towards an understanding of the microbial decomposition of archaeological bone in the burial environment. *Journal of Archaeological Science* 22: 165-174.
- Collins, M. J., Riley, M., Child, A. M., Turner-Walker, G., 1995. A basic mathematical simulation of the chemical degradation of ancient collagen. *Journal of Archaeological Science* 22, 175-83.
- Collins, M.J., Nielsen-Marsch, C.M., Hiller, J., Smith, C.I., Roberts, J.P., Prigodich, R.V., Wess, T.J., Csapò, J., Millard, A.R., Turner-Walker G., 2002. The survival of organic matter in bone: a review. *Archaeometry* 44, (3): 383-394.
- Croce, A.C., Bottirolì, G., 2014. Autofluorescence spectroscopy and imaging: a tool for biomedical research and diagnosis. *European Journal of Histochemistry* 58 (2461): 320-337.

474 Czermak, A., Schermelleh, L., Lee-Thorp, J.A., 2018, Imaging-assisted time-resolved dentine  
475 sampling to track weaning histories. *International Journal of Osteoarchaeology* 28: 535-  
476 541.

477 DeNiro, M.J., 1985. Post-mortem preservation and alteration of in vivo bone collagen isotope  
478 ratios in relation to palaeodietary reconstruction. *Nature* 317: 806-809.

479 Eyre, D.R., Paz, M.A., Gallop, P.M., 1984. Cross-linking in collagen and elastin. *Annual*  
480 *Review of Biochemistry* 53: 717-748.

481 Fernández-Crespo, T., Czermak, A., Lee-Thorp, J.A., Schulting, R.J., 2018. Infant and  
482 childhood diet at the passage tomb of Alto de la Huesera (north-central Iberia) from bone  
483 collagen and sequential dentine isotope composition. *International Journal of*  
484 *Osteoarchaeology* 28: 542-551.

485 Foreman, P.C. 1980: The excitation and emission spectra of fluorescent components of  
486 human dentine. *Archives of Oral Biology* 25 (10): 641-647.

487 France, C.A.M., Thomas, D.B., Doney, C.R., Madden, O., 2014. FT-Raman spectroscopy as a  
488 method for screening collagen diagenesis in bone. *Journal of Archaeological Science* 42:  
489 346-355.

490 Fujimori, E., 1989. Cross-linking and fluorescence changes of collagen by glycation and  
491 oxidation. *Biochimica Biophysica Acta* 998 (2): 105-110.

492 Eerkens, J.W., Berget, A.G., Bartelink, E.J., 2011. Estimating weaning and early childhood  
493 diet from serial micro-samples of dentin collagen. *Journal of Archaeological Science* 38:  
494 3101-3111.

495 Eerkens, J.W., Sullivan, K., Greenwald, A.M., 2016. Stable isotope analysis of serial samples  
496 of third molars as insight into inter- and intra-individual variation in ancient diet. *Journal*  
497 *of Archaeological Science* 53: 277-90.

498 Georgakoudi, I., Jacobson, B.C., Müller, M.G., Sheets, E.E., Badizadegan, K., Carr-Locke,  
499 D.L., Crum, Ch.P., Boone, Ch.W., Dasari, R.R., Van Dam, J., Feld, M.S., 2002.  
500 NAD(P)H and collagen as in vivo quantitative fluorescent biomarkers of epithelial  
501 precancerous changes. *Cancer Research* 62: 682-687.

502 Guiry, E.J., Hepburn, J.C., Richards, M.P., 2016. High-resolution serial sampling for nitrogen  
503 stable isotope analysis of archaeological mammal teeth. *Journal of Archaeological*  
504 *Science* 69: 21-28.

505 Hartles, R.L., Leaver, A.G., 1953. The fluorescence of teeth under ultraviolet irradiation.  
506 *Biochemical Journal* 54 (4): 632-638.

507 Hayase, K., Tsubota, H. (1985) Sedimentary humic acid and fulvic acid as fluorescent organic  
508 materials. *Geochimica et Cosmochimica Acta* 49 (1): 159-163.

509 Hedges, R.E.M., Millard, A.R., Pike, A., 1995. Measurements and relationships of diagenetic  
510 alteration of bone from three archaeological sites. *Journal of Archaeological Science* 22  
511 (2): 201-209.

512 Henderson, R.C., Lee-Thorp, J.A., Loe, L., 2014. Early life histories of the London poor  
513 using  $\delta^{13}\text{C}$  and  $\delta^{15}\text{N}$  stable isotope incremental dentine sampling. *American Journal of*  
514 *Physical Anthropology* 154 (4): 585-593.

515 Hoke, N., Burger, J., Weber, C., Benecke, N., Grupe, G., Harbeck, M., 2011. Estimating the  
516 chance of success of archaeometric analyses of bone: UV-induced bone fluorescence  
517 compared to histological screening. *Palaeogeography Palaeoclimatology Palaeoecology*  
518 310: 23-31.

519 Hollund, H.I., Jans, M.M.E., Collins, M.J., Kars, H., Joosten, I., Kars, S.M., 2012. What  
520 happened here? Bone histology as a tool in decoding the postmortem histories of



archaeological bone from Castricum, The Netherlands. *International Journal of Osteoarchaeology* 22: 537-548.

Hollund, H.I., Arts, N., Jans, M.M.E., Kars, H., 2015. Are teeth better? Histological characterization of diagenesis in archaeological bone – tooth pairs and a discussion of the consequences for archaeometric sample selection and analyses. *International Journal of Osteoarchaeology* 25: 901-911.

Jacob, E., Querci, D., Caparros, M., Barroso Ruiz, C., Higham, T., Deviese, T., 2018. Nitrogen content variation in archaeological bone and its implications for stable isotope analysis and radiocarbon dating. *Journal of Archaeological Science* 93: 68-73.

Jørkov, M.S., Heinemeier, J., Lynnerup, N. 2007. Evaluating bone collagen extraction methods for stable isotope analysis in dietary studies. *Journal of Archaeological Science* 34: 1824-1829.

Kendall, Ch., Høier Eriksen, A.M., Ioannis Kontopoulos, I., Collins, M.J., Turner-Walker, G., 2018. Diagenesis of archaeological bone and tooth. *Palaeogeography, Palaeoclimatology, Palaeoecology* 491: 21-37.

Kollias, N., Zonios, G., Stamatas, G.N. 2002. Fluorescence spectroscopy of skin. *Vibrational Spectroscopy* 28 (1): 17-23.

Van Klinken, G. J., 1999. Bone collagen quality indicators for palaeodietary and radiocarbon measurements. *Journal of Archaeological Science* 26, 687-95.

Klont, B., Damen, J. J. M. & ten Cate, J. M., 1991. Degradation of bovine incisor root collagen in an in vitro caries model. *Archives of Oral Biology* 36, 299-304.

König, K., Hibst, R., Meyer, H., Flemming, G., Schneckenburger, H., 1993. Laser-induced autofluorescence of carious regions of human teeth and caries-involved bacteria. *Proceedings of SPIE - The International Society for Optical Engineering* 2080(8)

König, K., Flemming, G., Hibst, R., 1999. Laser-induced autofluorescence spectroscopy of dental caries. *Cellular and Molecular Biology* 44 (8): 1293-1300.

Lakowicz, J.R., 2006. *Principles of Fluorescence Spectroscopy*, Third edition. Springer, Berlin.

Levallois, B., Terrer, E., Panayotov, Y., Salehi, H., Tassery, H., Tramini, P., Cuisinier, F., 2012. Molecular structural analysis of carious lesions using micro-Raman spectroscopy. *European Journal of Oral Science* 120 (5): 444-451.

Maggiano, C., T. Dupras, M. Schultz, J. Biggerstaff, 2009. Confocal laser scanning microscopy: a flexible tool for simultaneous polarization and threedimensional fluorescence imaging of archaeological compact bone, *Journal of Archaeological Science* 36 (10): 2392–2401.

Madden, O., Man Wai Chan, D., Dundon, M., France, C.A.M., 2018. Quantifying collagen quality in archaeological bone: Improving data accuracy with benchtop and handheld Raman spectrometers. *Journal of Archaeological Science: Reports* 18: 596-605.

Miles, C. A., Sionkowska, A., Hulin, S. L., Sims, T. J., Avery, N. C., and Bailey, A. J., 2000, Identification of an intermediate state in the helix-coil degradation of collagen by ultraviolet light, *Journal of Biological Chemistry*, 275, 33 014-20.

Pawlak, A.M., Glenn, J.V., Beattie, J.R., McGarvey, J.J., Stitt A.W. 2008. Advanced glycation as a basis for understanding retinal aging and non-invasive risk prediction. *Annals of the New York Academy of Sciences*, 1126 (1), 59-65.

Perry, A.J., Hefferren, J.J., 1973. Fluorescence of glycyl peptides and collagen degradation mixtures. *Calcified Tissue Research* 11 (3): 265-268.

Sandberg, P.A., Sponheimer, M., Lee-Thorp, J.A., van Gerven, D., 2014. Intra-tooth stable isotope analysis of dentine: a step toward addressing selective mortality in the

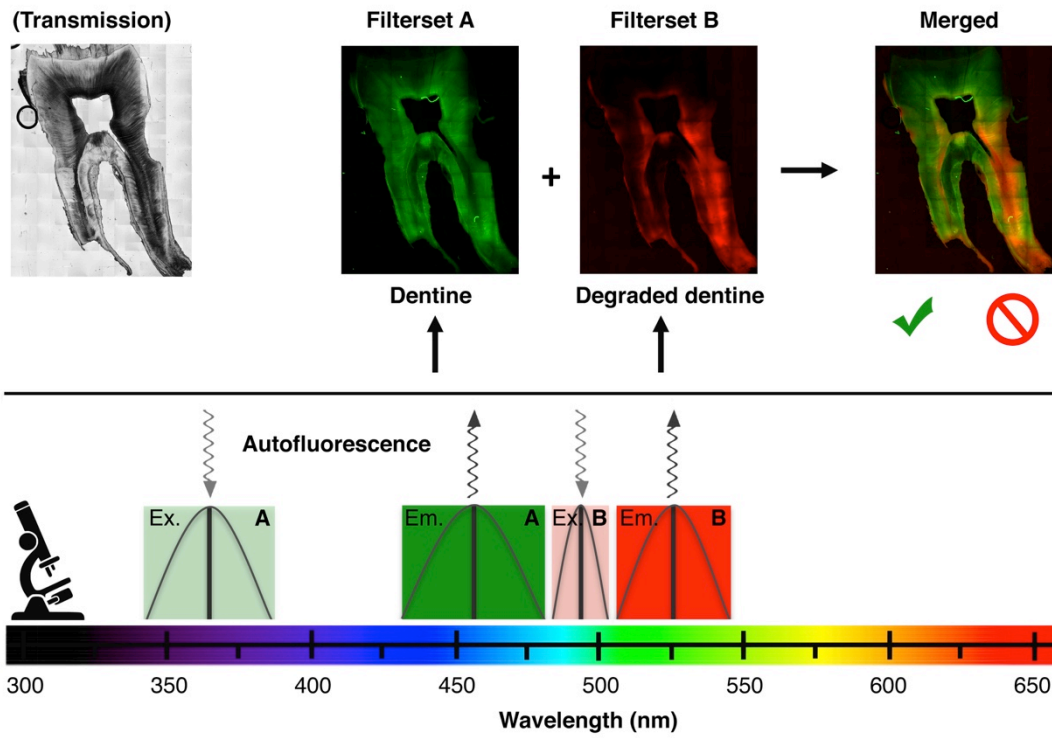
- reconstruction of life history in the archaeological record. *American Journal of Physical Anthropology* 55: 281-293.
- Schindelin, J., Arganda-Carreras, I., Frise, E., Kaynig, V., Longair, M., Pietzsch, T., Preibisch, S., Rueden, C., Saalfeld, S., Schmid, B., Tinevez, J.Y., White, D.J., Hartenstein, V., Eliceiri, K., Tomancak, P., Cardona, A., 2012. Fiji: an open-source platform for biological-image analysis. *Nature Methods* 9 (7): 676-682.
- Schroeder, H.E., 2000. *Orale Strukturbiologie / Oral Structural Biology* (German version). Thieme Verlag Stuttgart.
- Sealy J., Johnson, M., Richards, M.P., Nehlich, O., 2014. Comparison of two methods of extracting bone collagen for stable carbon and nitrogen isotope analysis: comparing whole bone demineralization with gelatinization and ultrafiltration. *Journal of Archaeological Science* 47: 64-69.
- Szpak, P., 2011. Fish bone chemistry and ultrastructure: implications for taphonomy and stable isotope analysis, *Journal of Archaeological Science* 38: 3358-3372.
- Szpak, P., Krippner, K., Richards, M.P. 2017. Effects of Sodium Hydroxide Treatment and Ultrafiltration on the Removal of Humic Contaminants from Archaeological Bone. *International Journal of Osteoarchaeology* 27 (6): 1070-1077.
- Stübel, H., 1911. Die Fluoreszenz tierischer Gewebe in ultraviolettem Licht. *Pflüger's Archiv für die gesamte Physiologie des Menschen und der Tiere* (now *European Journal of Physiology*) 142 (1-2): 1-14.
- Turner-Walker, G., Syversen, U., 2002. Quantifying histological changes in archaeological bones using BSE – SEM image analysis. *Archaeometry* 44: 461-468.
- Turner-Walker, G., Nielsen-Marsh, C.M., Syversen, U., Kars, H., Collins, M.J., 2002. Sub-micron spongiform porosity is the major ultra-structural alteration occurring in archaeological bone. *International Journal of Osteoarchaeology* 12: 407-414.
- Van der Haas V.M., Garvie-Lok S., Bazaliiski V.I., Weber A.W., Evaluating sodium hydroxide usage for stable isotope analysis of prehistoric human tooth dentine, *J. Arch. Sci. Reports* 20, 2018, 80–86. doi.org/10.1016/j.jasrep.2018.04.013.

## Figure captions

**Fig. 1.** Dual-colour autofluorescence imaging of tooth thin sections. A. Autofluorescence images of modern, surgically extracted control samples (Filterset A: pseudo-coloured green; Filterset B: pseudo-coloured red). Intense autofluorescence with Filterset A, no signal with Filterset B, except for regions with caries lesions (arrows, right panel). B. Differential dual-colour autofluorescence images of archaeological samples (columns 1-3: Filterset A, Filterset B and merged) highlight varying levels of degradation indicated by changes from green to red in the merged images: little overall degradation (tooth A), varying stages of degradation in partially decayed areas around the right root canal (tooth B), the pulp cavity (tooth C) or parts damaged by dental neck caries (tooth D) and severe decay accompanied by material loss (tooth E, dark areas, arrows). Photographs of corresponding demineralized tooth halves with degraded areas characterised by different colour and structure (column 4).

**Fig. 2.** Microsampling and CN-isotope analysis results. A. Microsampling using a Ø 1.0 mm biopsy punch shown as schematic (left) and on an example tooth, before (middle) and after (right) punching. B. Sampling areas for isotope analysis in sound and degraded areas, indicated by red cycles in the corresponding dual-colour autofluorescence imaged thin section. According to the colour displayed in the merged fluorescence images four fluorescence stages were assigned: (1) green; (2) yellow; (3) orange; (4) red. C. Table of isotope analysis results:  $\delta^{15}\text{N}$  and  $\delta^{13}\text{C}$  values, C/N-ratio, %C and %N and sample weight gained from each biopsy sample and the corresponding colour stage is displayed.

**Fig. 3.** Collagen amount, C/N ratios, %C and %N in samples from different fluorescence stages. A. C/N ratios compared to collagen amount, %N (wt) and %C (wt), and proportion of %C to %N of samples taken from regions of different preservation levels. B. Collagen amount (sample weight), C/N ratios, %C and %N in different preservation stages. Brackets and asterisks indicate differences between fluorescence stages: \*  $p \leq 0.05$ ; \*\*  $p \leq 0.01$ .



630  
631  
632

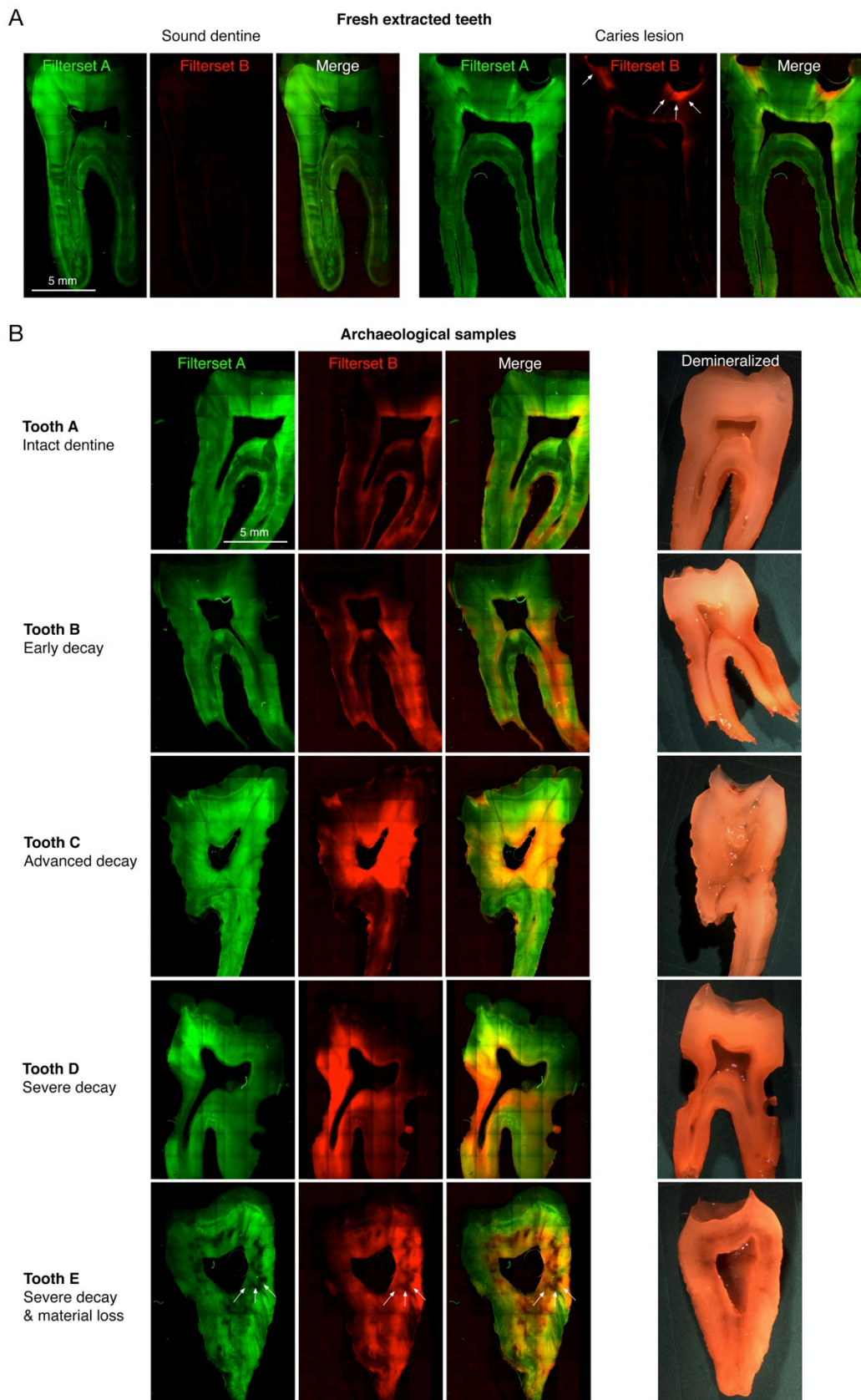


**Figure 1**

633  
634

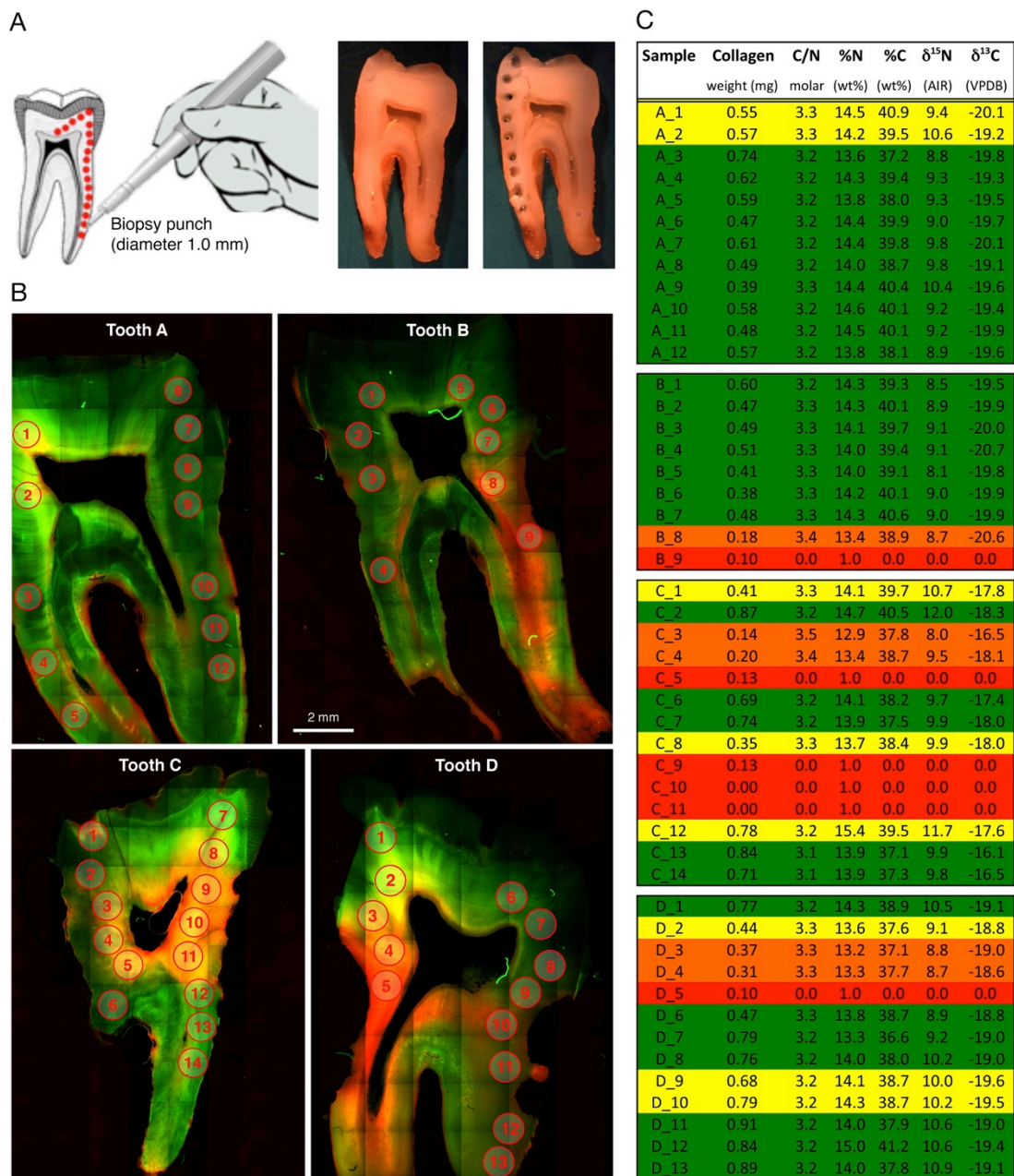
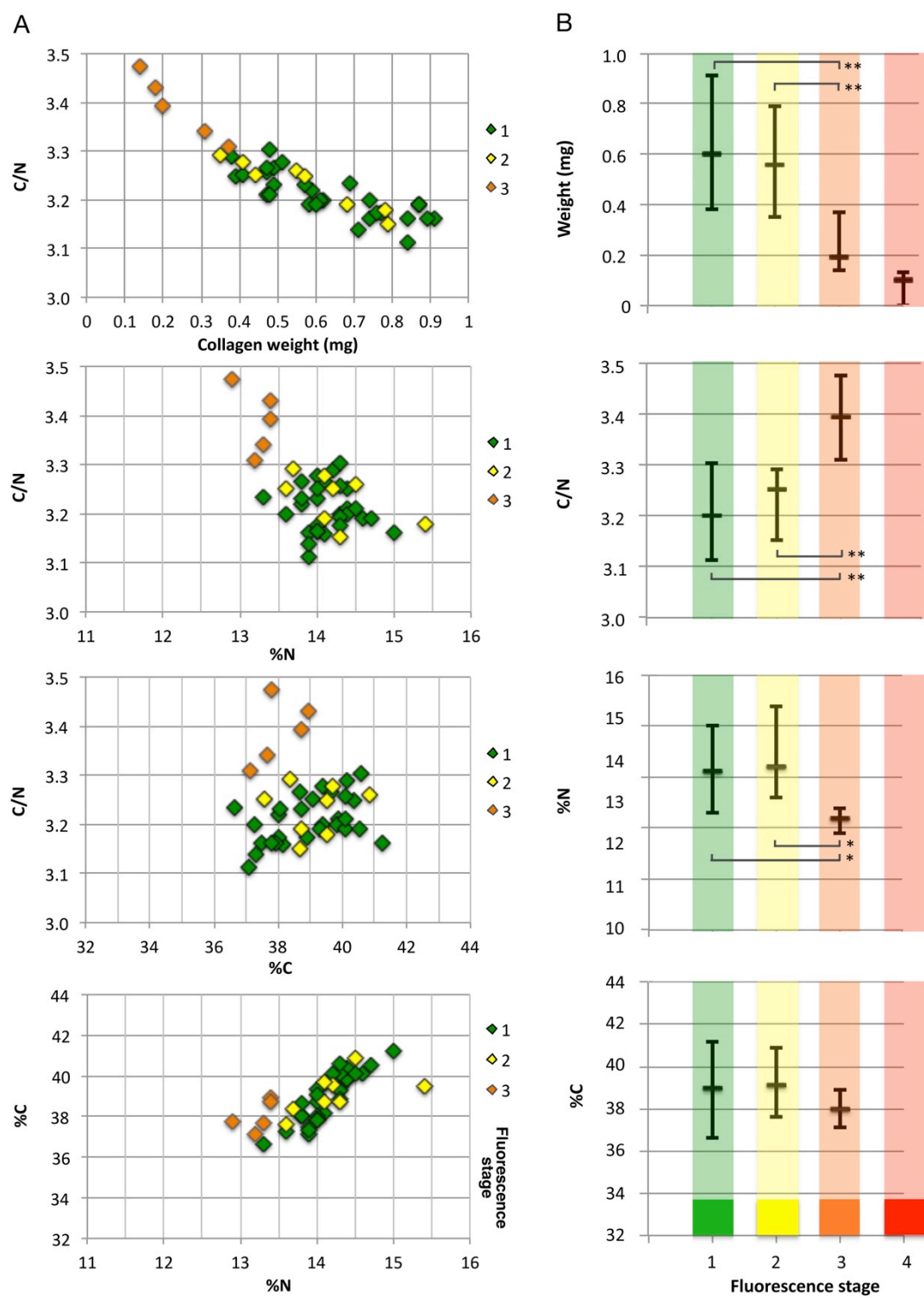


Figure 2





**Figure 3**

## SUPPLEMENTARY MATERIAL

### Supplementary S1. Additional sodium hydroxide (NaOH) treatment

#### *Introduction*

Alkali treatment, which is usually applied to remove humic contaminants, can decrease collagen yield (Szpak et al., 2017). Since the sample teeth did not show any apparent signs of humic acid contamination, i.e. yellow-brown colouring, and in order to minimize collagen loss, a NaOH-step in the collagen extraction process of dentine microsamples was omitted in this study.

Humics are dark coloured substances present in soil derived from decaying organic matter. Compared to collagen, they are carbon rich and nitrogen poor, with low  $\delta^{13}\text{C}$  values. In the burial environment they can infiltrate bone and teeth and link to collagen. Contamination with humic substance can therefore potentially alter results of isotope analyses by increasing %C and C/N ratios (Szpak et al. 2017). Although some studies include a sodium hydroxide treatment (Eerkens et al. 2011, 2016; Burt and Garvie-Lok 2013), it is currently not standard in dentine microsampling protocols (e.g. Henderson et al. 2014; Sandberg et al. 2014; Beaumont and Montgomery, 2016; Fernández-Crespo et al., 2018). Van der Haas et al. (2018) recently included a NaOH-step on their microsamples and demonstrated that a 6 h base-wash does not cause material loss in archaeological microsamples.

In this study, autofluorescence is used to differentiate intact and degraded collagen, using two filter-sets with different excitation/emission ranges. Degraded collagen and humics are fluorescent under similar excitation/emission wavelengths (excitation 470-510 nm, emission 490-566 nm, Filterset B). To exclude humics as potential cause of fluorescence, we conducted an additional experiment on the same teeth, comparing the weight of samples taken from well-preserved and degraded areas, with and without base-wash.

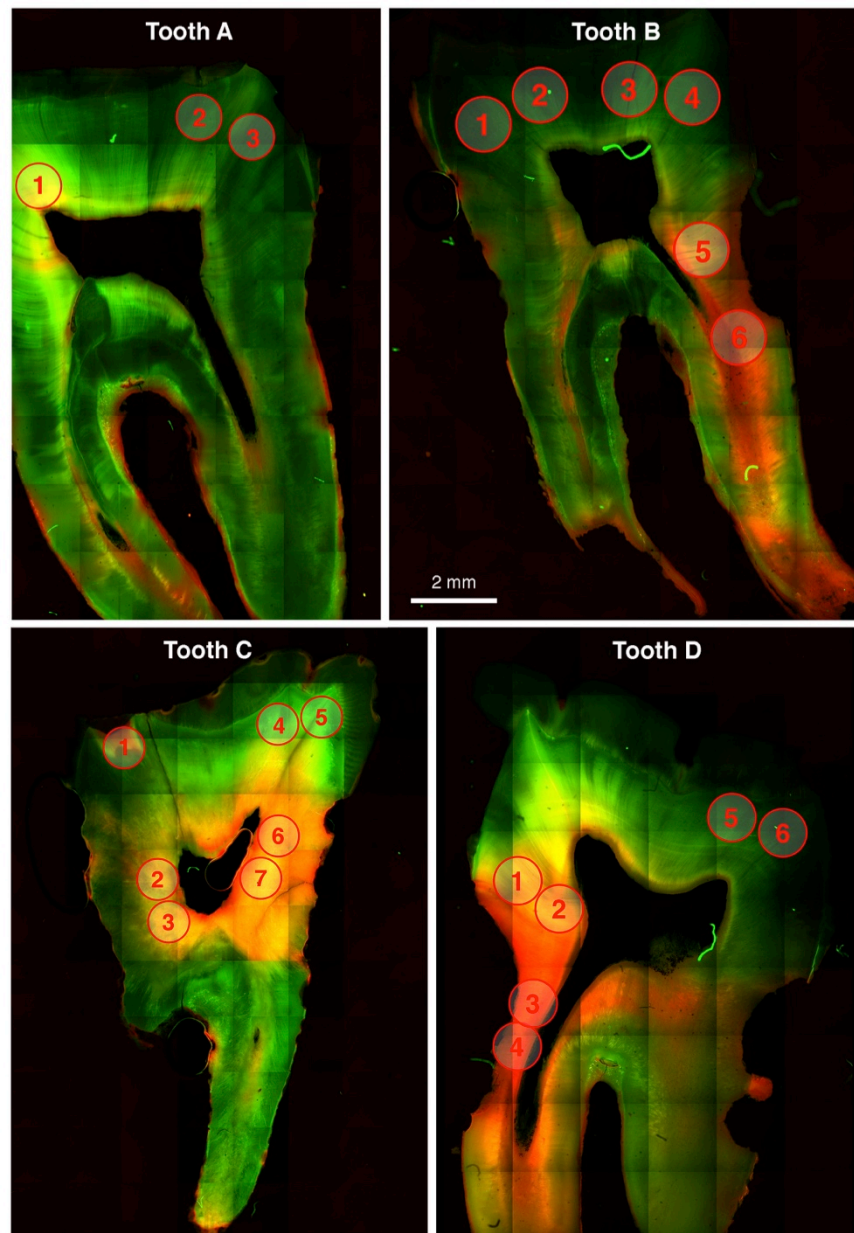
#### *Material and Method*

The corresponding tooth halves of the four archaeological samples were used for this additional NaOH experiment. Tooth halves were demineralized in 0.5 M hydrochloric acid (HCl) solution at 4°C. The acid was changed every other day until the teeth appeared flexible, indicating complete decalcification. Tooth samples were rinsed and soaked in deionized water, changing the water every day until pH was neutral (for three days). Demineralized tooth halves were sectioned longitudinally to obtain a ~1.5 mm thick slice. Small dentine micro-cylinders of 1 mm diameter and ~1.5 mm length were taken using a KAI Medical biopsy-punch with plunger (Fig. 2a, main text). Fluorescence images of the corresponding thin section were used as an optical reference to track different areas of collagen preservation and previous sampled areas (Fig. S1). Dentine micro-cylinders were soaked in 0.1 M NaOH for 3 x 20 min (Szpak 2017) and then rinsed 3x and soaked in deionized water for two days, changing the water every day. When pH-neutral, micro-cylinders were lyophilized for 4-6 h and weighed after freeze-drying.



## Results

Since the corresponding tooth halves were thinner than those previously used for isotope analysis thus, no samples were taken from the lower root area. It was possible to take 22 microsamples in total. Nine samples could be taken in duplicate, five from well-preserved areas (green: A2,3; B1,2 and B3,4; C4,5; D5,6), two from areas of advanced (orange: C2,3; D1,2) and two from areas of severe decay (red: C2,3; D3,4). Only two single samples could be taken from areas early decay (yellow: A1; C1 caries), and one each from orange (B5) and red (B6). In this case, we used samples, taken from the opposite tooth half for isotope analysis, as an approximate correspondent (Fig. S1; Tab. S1).



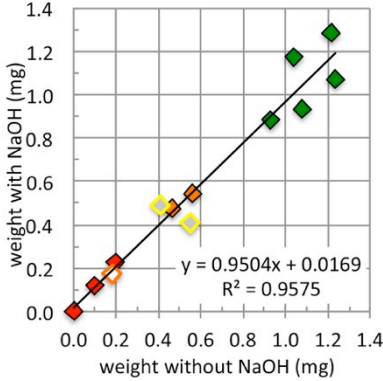
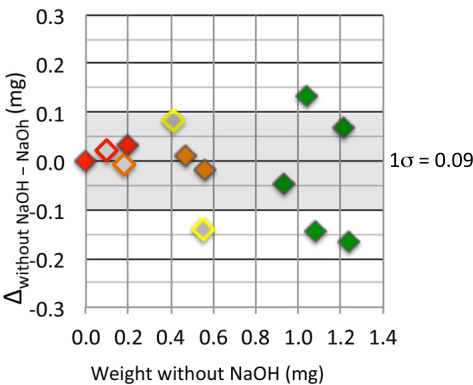
**Supplementary Fig. S1.** Microsamples taken for NaOH-treatment. “Duplicate” samples are located next to each other, for single samples, data from corresponding tooth half were used (see Fig. 2, Main Manuscript).

## Supplementary References

- Beaumont, J., Montgomery, J., 2016. The Great Irish Famine: Identifying starvation in the tissues of victims using stable isotope analysis of bone and incremental dentine collagen. *PLoS one*: 11(8): e0160065.
- Burt N.M., Garvie-Lok S., A new method of dentine microsampling of deciduous teeth for stable isotope ratio analysis, *J. Archaeol. Sci.* 40, 2013, 3854–3864.
- Eerkens, J.W., Berget, A.G., Bartelink, E.J., 2011. Estimating weaning and early childhood diet from serial micro-samples of dentin collagen. *J. Arch. Sci.* 38: 3101-3111.
- Eerkens, J.W., Sullivan, K., Greenwald, A.M., 2016. Stable isotope analysis of serial samples of third molars as insight into inter- and intra-individual variation in ancient diet. *J. Arch. Sci.* 53: 277-90.
- Fernández-Crespo, T., Czermak, A., Lee-Thorp, J.A., Schulting, R.J., 2018. Infant and childhood diet at the passage tomb of Alto de la Huesera (north-central Iberia) from bone collagen and sequential dentine isotope composition. *Int. J. Osteoarch.* 28: 542-551.
- Henderson, R.C., Lee-Thorp, J.A., Loe, L., 2014. Early life histories of the London poor using  $\delta^{13}\text{C}$  and  $\delta^{15}\text{N}$  stable isotope incremental dentine sampling. *Am. J. Phys. Anth.* 154 (4): 585-593.
- Sandberg, P.A., Sponheimer, M., Lee-Thorp, J.A., van Gerven, D., 2014. Intra-tooth stable isotope analysis of dentine: a step toward addressing selective mortality in the reconstruction of life history in the archaeological record. *American Journal of Physical Anthropology* 55: 281-293.
- Szpak, P., Krippner, K., Richards, M.P. 2017. Effects of Sodium Hydroxide Treatment and Ultrafiltration on the Removal of Humic Contaminants from Archaeological Bone. *International Journal of Osteoarchaeology* 27 (6): 1070-1077.
- Van der Haas V.M., Garvie-Lok S., Bazaliiskii V.I., Weber A.W., Evaluating sodium hydroxide usage for stable isotope analysis of prehistoric human tooth dentine, *J. Arch. Sci. Reports* 20, 2018, 80–86. doi.org/10.1016/j.jasrep.2018.04.013.

**Supplementary Table S1.** Sample weight with and without NaOH-treatment. Samples labelled with asterisks were taken for isotope analysis from the corresponding tooth halve. Colour is referring to sample areas: green = well preserved; yellow = early decay; orange = advanced decay; red = severe decay.

Sample	without NaOH weight (mg)	Duplicate	with NaOH weight (mg)	$\Delta_{\text{withoutNaOH-NaOH}}$
NaOH_B_1	1.24	NaOH_B_2	1.07	-0.16
NaOH_C_4	1.21	NaOH_C_5	1.28	0.07
NaOH_A_2	1.08	NaOH_A_3	0.93	-0.14
NaOH_D_3	1.04	NaOH_D_6	1.17	0.13
NaOH_B_3	0.93	NaOH_B_4	0.88	-0.05
A_1*	0.55	NaOH_A_1	0.41	-0.14
C_1*	0.41	NaOH_C_1_caries	0.49	0.08
NaOH_D_1	0.56	NaOH_D_2	0.54	-0.02
NaOH_C_2	0.47	NaOH_C_3	0.48	0.01
B_8*	0.18	NaOH_B_5	0.17	-0.01
NaOH_C_6	0.20	NaOH_C_7	0.23	0.03
B_9*	0.10	NaOH_B_6	0.12	0.02
NaOH_D_3	0.00	NaOH_D_4	0.00	0.00
Average				-0.01
1 $\sigma$				0.09
max				0.13
min				-0.16



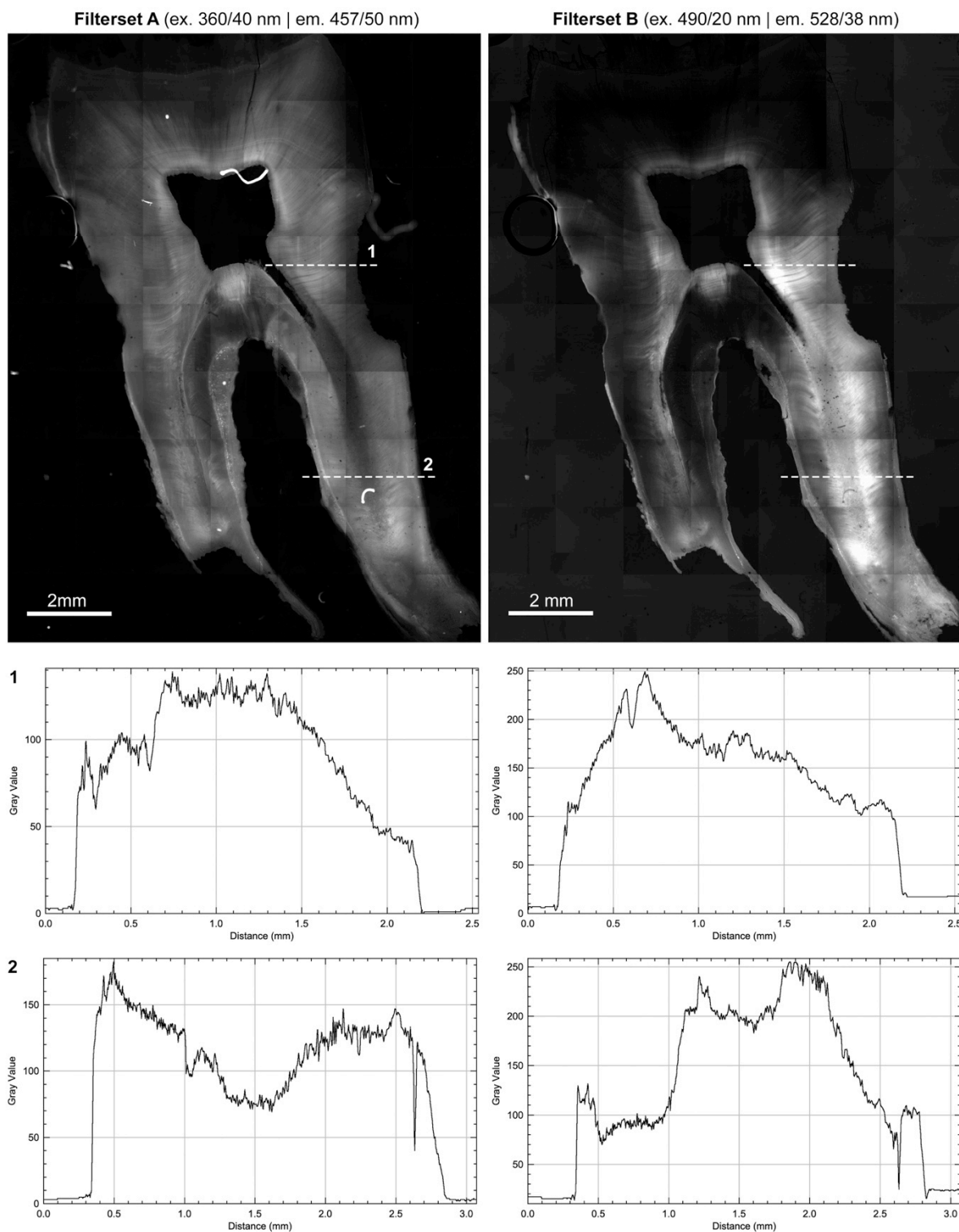
**Supplementary Fig. S2.** Difference between weights of samples with NaOH-treatment compared to weight of equivalent samples without NaOH-treatment (unfilled diamonds represent samples without direct duplicate). Yellow unfilled outlier: caries lesion (tooth C, sample 1)

**Supplementary Fig. S3.** Sample weight of equivalent samples with and without NaOH-treatment (unfilled diamonds represent samples without direct duplicate).

No significant weight loss was observed between samples after NaOH-treatment and untreated samples at areas representing degraded or contaminated areas (yellow and orange). This confirms, that no humic substances are present in this samples. The results also confirm, that NaOH-treatment can be applied on microsamples without significant material loss. A potential material loss would most likely be caused by the “loss” of humics.

745  
746

## Supplementary S2. Intensity profile plot analysis



747  
748  
749  
750  
751  
752  
753

**Supplementary Fig. S4.** Intensity profile plot analysis. Tooth B autofluorescence intensities detected with Filterset A (left column) and Filterset B (right column) displayed separately. Profile plots of fluorescence intensity along lines 1 and 2 highlight a variable degree of anti-correlation of intact (left column) versus degraded (right column) collagen.

## Supplementary S2. Calibration and Analytical Accuracy

Reference samples of alanine and in-house cow and seal collagen standards were used to check the quality of the runs and to calibrate the results. The  $\delta^{13}\text{C}$  and  $\delta^{15}\text{N}$  measurements were calibrated using a two-point calibration curve using the internal cow and seal collagen standards. Analytical reproducibility is  $\pm 0.22\%$  for  $\delta^{15}\text{N}$  and  $\pm 0.16\%$  for  $\delta^{13}\text{C}$ , based on multiple replicates of the internal laboratory standard.

**Supplementary Table S2.** Standard reference materials used for calibration of  $\delta^{13}\text{C}$  relative to VPDB and  $\delta^{15}\text{N}$  relative to AIR for internal accuracy and precision.

Standard	Material	$\delta^{15}\text{N}$ (‰, AIR)	$\delta^{13}\text{C}$ (‰, VPDB)
IAEA-600	Caffeine	$+1.0 \pm 0.2$	$-27.8 \pm 0.1$
IRM-1	Alanine	$-1.3 \pm 0.1$	$-26.9 \pm 0.1$
IRM-2	Modern cow bone collagen	$+7.8 \pm 0.2$	$-24.3 \pm 0.2$
IRM-3	Marine seal bone collagen	$+16.6 \pm 0.2$	$-12.0 \pm 0.2$

**Supplementary Table S3.** Mean and standard deviation of check standards for all analytical sessions containing data presented in this paper. Weight groups: (1) 0.2-0.4; (2) 0.5-0.6; (3) 0.7-0.9

Run ID	Weight group	Standard	N	$\delta^{15}\text{N}$ (‰, AIR)	$\delta^{13}\text{C}$ (‰, VPDB)
Run 1 <sub>100</sub>	3	IRM-1 Alanine	15	$-1.48 \pm 0.20$	$-27.06 \pm 0.08$
Run 1 <sub>100</sub>	3	IRM-2 Cow	8	$7.56 \pm 0.15$	$-24.49 \pm 0.03$
Run 1 <sub>100</sub>	3	IRM-3 Seal	8	$16.87 \pm 0.20$	$-12.34 \pm 0.07$
Run 2 <sub>50</sub>	2	IRM-1 Alanine	9	$-1.57 \pm 0.27$	$-27.08 \pm 0.26$
Run 2 <sub>50</sub>	2	IRM-2 Cow	4	$7.81 \pm 0.09$	$-24.34 \pm 0.08$
Run 2 <sub>50</sub>	2	IRM-2 Seal	4	$16.98 \pm 0.26$	$-11.82 \pm 0.16$
Run 3 <sub>50</sub>	1	IRM-1 Alanine	9	$-1.72 \pm 0.19$	$-27.21 \pm 0.09$
Run 3 <sub>50</sub>	1	IRM-2 Cow	4	$7.89 \pm 0.12$	$-24.48 \pm 0.15$
Run 3 <sub>50</sub>	1	IRM-2 Seal	4	$16.67 \pm 0.22$	$-12.54 \pm 0.06$
Run 3 <sub>50</sub>	1	IAEA-600 Caffeine	4	$0.92 \pm 0.18$	$-27.64 \pm 0.22$
Run 4 <sub>100</sub>	3	IRM-1 Alanine	16	$-1.63 \pm 0.28$	$-27.13 \pm 0.23$
Run 4 <sub>100</sub>	3	IRM-2 Cow	8	$7.67 \pm 0.23$	$-24.35 \pm 0.04$
Run 4 <sub>100</sub>	3	IRM-3 Seal	8	$16.13 \pm 0.17$	$-12.34 \pm 0.06$
Run 5 <sub>100</sub>	3	IRM-1 Alanine	16	$-1.47 \pm 0.23$	$-27.12 \pm 0.23$
Run 5 <sub>100</sub>	3	IRM-2 Cow	8	$7.76 \pm 0.05$	$-24.49 \pm 0.02$
Run 5 <sub>100</sub>	3	IRM-3 Seal	8	$16.43 \pm 0.09$	$-12.49 \pm 0.05$

**Supplementary Table S4.** Mean and standard deviation all standards used.

Standard	Material	N	$\delta^{15}\text{N}$ (‰, AIR)	$\delta^{13}\text{C}$ (‰, VPDB)
IRM-1	Alanine	80	$-1.51 \pm 0.22$	$-27.12 \pm 0.17$
IRM-2	Modern cow bone collagen	32	$+7.69 \pm 0.19$	$-24.44 \pm 0.10$
IRM-3	Marine seal bone collagen	32	$+16.66 \pm 0.24$	$-12.33 \pm 0.22$

# Supplementary S3. Additional data and figures

## Supplementary Table S5. Carbon and nitrogen stable isotope measurements.

Sample	Weight	N (Sam) $\mu\text{g}$	%N	$^{15}\text{N}$ (Sam) DeltaAir	C (Sam) $\mu\text{g}$	%C	$^{13}\text{C}$ (Sam) DeltaPDB	C/N molar	$\delta^{15}\text{N}$ AIR	$\delta^{13}\text{C}$ VPDB
A_1	0.55	96.4	14.5	9.3	269.7	40.9	-20.5	3.3	9.4	-20.1
A_2	0.57	131.4	14.2	10.3	365.3	39.5	-19.6	3.3	10.6	-19.2
A_3	0.74	135.7	13.6	8.8	330.7	37.2	-20.2	3.2	8.8	-19.8
A_4	0.62	107.1	14.3	9.2	293.2	39.4	-19.7	3.2	9.3	-19.4
A_5	0.59	135.7	13.8	9.2	269.2	38.0	-19.9	3.2	9.3	-19.5
A_6	0.47	81.8	14.4	9.0	224.8	39.9	-20.1	3.2	9.0	-19.7
A_7	0.61	135.7	14.4	9.8	291.5	39.8	-20.3	3.2	9.8	-20.1
A_8	0.49	82.2	14.0	9.6	227.8	38.7	-19.5	3.2	9.8	-19.1
A_9	0.39	67.9	14.4	10.2	189.0	40.4	-20.0	3.3	10.4	-19.6
A_10	0.58	102.1	14.6	9.2	279.2	40.1	-19.8	3.2	9.2	-19.4
A_11	0.48	83.9	14.5	9.1	231.0	40.1	-20.3	3.2	9.2	-19.9
A_12	0.57	135.7	13.8	8.9	260.2	38.1	-20.0	3.2	8.9	-19.6
B_1	0.60	135.7	14.3	8.6	283.0	39.3	-19.8	3.2	8.5	-19.5
B_2	0.47	135.7	14.3	8.9	226.2	40.1	-20.2	3.3	8.9	-19.9
B_3	0.49	135.7	14.1	9.1	233.1	39.7	-20.2	3.3	9.1	-20.0
B_4	0.51	135.7	14.0	9.1	241.0	39.4	-20.9	3.3	9.1	-20.7
B_5	0.41	135.7	14.0	8.2	192.2	39.1	-20.0	3.3	8.2	-19.8
B_6	0.38	135.7	14.2	9.0	183.0	40.1	-20.2	3.3	9.0	-19.9
B_7	0.48	135.7	14.3	9.0	233.9	40.6	-20.1	3.3	9.0	-19.9
B_8	0.18	135.7	13.4	8.7	84.1	38.9	-20.8	3.4	8.7	-20.6
C_1	0.41	135.7	14.1	10.6	195.2	39.7	-17.7	3.3	10.7	-17.8
C_2	0.87	135.7	14.7	12.0	423.1	40.5	-18.3	3.2	12.1	-18.3
C_3	0.14	135.7	12.9	7.9	63.5	37.8	-16.4	3.4	8.0	-16.5
C_4	0.20	135.7	13.4	9.4	92.9	38.7	-18.1	3.4	9.5	-18.2
C_6	0.69	135.7	14.1	9.7	316.0	38.2	-17.4	3.2	9.7	-17.4
C_7	0.74	135.7	13.9	9.9	332.7	37.5	-18.0	3.2	9.9	-18.0
C_8	0.35	135.7	13.7	9.9	161.2	38.4	-18.0	3.3	9.9	-18.0
C_12	0.78	135.7	14.4	11.6	369.8	39.5	-17.5	3.2	11.7	-17.6
C_13	0.84	135.7	13.9	9.9	373.9	37.1	-16.1	3.1	9.9	-16.1
C_14	0.71	135.7	13.9	9.8	317.9	37.3	-16.5	3.1	9.8	-16.5
D_1	0.77	135.7	14.3	10.4	359.3	38.9	-19.3	3.2	10.5	-19.1
D_2	0.44	135.7	13.6	9.1	198.5	37.6	-19.0	3.2	9.2	-18.8
D_3	0.37	135.7	13.2	8.8	164.9	37.1	-19.2	3.3	8.8	-19.0
D_4	0.31	135.7	13.3	8.7	140.1	37.7	-18.9	3.3	8.7	-18.6
D_6	0.47	135.7	13.8	8.9	218.1	38.7	-19.1	3.3	8.9	-18.9
D_7	0.79	135.7	13.3	9.2	347.1	36.6	-19.3	3.2	9.2	-19.0
D_8	0.76	135.7	14.0	10.2	346.5	38.0	-19.3	3.2	10.2	-19.0
D_9	0.68	135.7	14.1	10.0	316.0	38.7	-19.8	3.2	10.0	-19.6
D_10	0.79	135.7	14.3	10.2	366.8	38.7	-19.7	3.2	10.2	-19.5
D_11	0.91	135.7	14.0	10.5	414.0	37.9	-19.2	3.2	10.6	-19.0
D_12	0.84	135.7	15.0	10.5	415.7	41.2	-19.6	3.2	10.6	-19.4
D_13	0.89	135.7	14.0	10.8	403.7	37.8	-19.4	3.2	10.9	-19.1

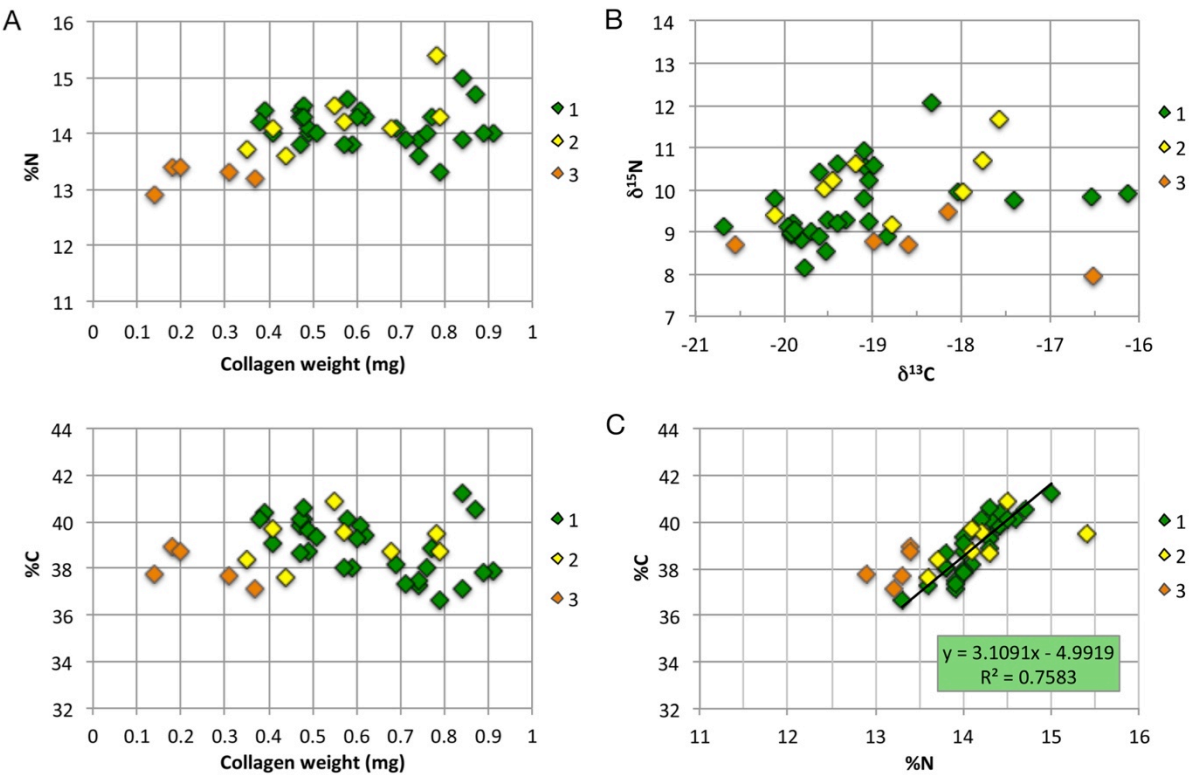
**Supplementary Table S6.** Mean, minimum and maximum of collagen weight, %N, %C, C/N,  $\delta^{15}\text{N}$  and  $\delta^{13}\text{C}$  of samples from different fluorescence stages (1: green, intact; 2: yellow, early decay; 3: orange, advanced decay; 4: red, severe decay).

Sample	Collagen weight (mg)	%N (wt%)	%C (wt%)	C/N molar	$\delta^{15}\text{N}$ (AIR)	$\delta^{13}\text{C}$ (VPDB)	Fluorescence stage
Mean	0.63	14.1	39.0	3.2	9.6	-19.2	1
Min	0.38	13.3	36.6	3.1	8.1	-20.7	
Max	0.91	15.0	41.2	3.3	12.0	-16.1	
Mean	0.57	14.2	39.1	3.2	10.2	-18.8	2
Min	0.35	13.6	37.6	3.2	9.1	-20.1	
Max	0.79	15.4	40.9	3.3	11.7	-17.6	
Mean	0.24	13.2	38.0	3.4	8.7	-18.6	3
Min	0.14	12.9	37.1	3.3	8.0	-20.6	
Max	0.37	13.4	38.9	3.5	9.5	-16.5	
Mean	0.08	0.0	0.0	0.0	0.0	0.0	4
Min	0.00	0.0	0.0	0.0	0.0	0.0	
Max	0.13	0.0	0.0	0.0	0.0	0.0	

**Supplementary Table S7.** Median, 1<sup>st</sup> and 2<sup>nd</sup> standard deviation of collagen weight, %N, %C, C/N,  $\delta^{15}\text{N}$  and  $\delta^{13}\text{C}$  of samples from different fluorescence stages (1: green, intact; 2: yellow, early decay; 3: orange, advanced decay).

Sample	Collagen weight (mg)	%N (wt%)	%C (wt%)	C/N molar	$\delta^{15}\text{N}$ (AIR)	$\delta^{13}\text{C}$ (VPDB)	Fluorescence stage
Median	0.60	14.1	39.1	3.2	9.3	-19.4	1
1 $\sigma$	0.16	0.3	1.2	0.0	0.8	1.0	
2 $\sigma$	0.33	0.7	2.5	0.1	1.7	2.0	
Median	0.56	14.2	39.1	3.3	10.1	-19.0	2
1 $\sigma$	0.17	0.6	1.0	0.1	0.8	0.9	
2 $\sigma$	0.33	1.1	2.0	0.1	1.6	1.9	
Median	0.20	13.3	37.8	3.4	8.7	-18.6	3
1 $\sigma$	0.10	0.2	0.8	0.1	0.5	1.5	
2 $\sigma$	0.19	0.4	1.5	0.1	1.1	2.9	

Supplementary S4. Additional data plots



**Supplementary Fig. S5.** Isotope measurement data taken from areas of different fluorescence stages. Samples taken from red areas contained 0.1 mg or less collagen and could not be measured. A. %N and %C compared to the collagen weight of samples taken from regions of different fluorescence stages. B. Regression line for %C and %N of samples from well-preserved areas (green fluorescence). Data shown in bottom diagram of Fig. 3, main manuscript. C.  $\delta^{15}\text{N}$  and  $\delta^{13}\text{C}$  results from samples taken from different fluorescence areas.